

Support of The Return Airway In The Lower Slice of A Thick Coal Seam

JiaXin Guo

School of Energy Science and Engineering, Henan Polytechnic University, Jiaozuo, Henan 454003, China

Email: 2369345064@qq.com

How to cite this paper: Guo, J. X. (2026). Support of the return airway in the lower slice of a thick coal seam. *Academic Journal of Emerging Technologies*, 3(1), 71–82. ISSN Print: 3104-4417; ISSN Online: 3104-4425.

<https://doi.org/10.63313/AJET.9055>

Published: 2026-05-11

Copyright © 2026 by author(s) and Erytis Publishing Limited.

This work is licensed under the Creative Commons Attribution International License (CC BY 4.0).

<http://creativecommons.org/licenses/by/4.0/>



Abstract

To address the support challenges of lower-seam gate roads under conditions of thick coal seam slicing mining and village-subjacent coal extraction, this study investigates the 52204 tailgate at WulanSetai Coal Mine. The gate road is situated 6 m inward from the solid coal boundary of the upper-seam 52113 goaf. Based on Protodyakonov's pressure arch theory, a mechanical source analysis model for the tailgate was established, and support effectiveness was evaluated using FLAC3D numerical simulation. Results indicate that due to the gate road's position beneath the goaf, I-beam steel sets with a spacing of 450 mm are recommended. Additionally, to counteract the lateral load exerted by the boundary solid coal on the gate road ribs, supplementary rock bolts were installed on the pillar-side rib. These bolts are positioned at heights of 1.8 m, 2.7 m, and 3.3 m above the floor, thereby significantly enhancing the overall stability of the gate road.

Keywords

Ultra-Thick Coal Seam; Remnant Coal Body; Lower-Seam Gate Road Layout; Protodyakonov's Pressure Arch; I-Beam Support

1. Introduction

The Wulanseitai Coal Mine mainly extracts the 5-2 coal seam with an average thickness of 7.8 m, which is classified as a thick coal seam. In the compound area of the north wing, slicing mining is adopted. The upper slice has been fully extracted, but some coal remains unmined beneath a village due to surface subsidence constraints. The return airway of the 52204 working face in the lower slice is arranged with an inner stagger of 6 m into the solid coal beside the goaf boundary of the upper-slice 52113 working face, and a 1 m thick coal layer is left between the two working faces to serve as an artificial false roof. To improve the resource recovery rate, a strip-filling mining method is planned to first extract the triangular coal pillar trapped under the village. One end of the filling strip opens into the

52204 return airway, so this airway simultaneously serves both the backfill mining district and the 52204 working face, resulting in a long service period and multiple factors affecting its stability. For thick coal seams mined by slicing, the lower-slice return airway can be arranged in three typical patterns: inner stagger, outer stagger, and overlapping layout. Among these, the inner-stagger arrangement places the roadway in the stress-relief zone beneath the overlying goaf, which is favorable for roadway stability and support. Taking the return airway of the 52204 working face as the research subject, this study employs theoretical analysis and numerical simulation to reveal the floor stress distribution characteristics under the overlying remnant boundary coal pillar, thereby providing a theoretical basis for the support scheme of this roadway.

2. Mechanism of roadway support under fractured surrounding rock conditions

2.1. Study on The Support Scheme of The Return Airway

(1) Affected by the mining activities of the upper-slice working face, fractures are widely developed in the coal mass of the lower slice, leading to a reduction in the overall strength of the rock mass and compromised integrity. These fractures cut the rock mass into relatively small blocks, causing it to behave mechanically in a manner close to that of a granular medium. However, a certain degree of cohesion still remains between the rock blocks. Therefore, this type of rock mass can be regarded as a Protodyakonov pressure[1-2] arch formed in a quasi-granular medium with residual cohesion.

(2) After the mining of the upper-slice working face, part of the rock mass above the roadway roof collapses under its own weight, forming a goaf. When the lower-slice return airway, located beneath this goaf, is excavated, the load generated by the caved gangue in the goaf will act on the roadway roof. Since the caved gangue in the goaf can be regarded as a quasi-granular medium with residual cohesion, it is capable of forming a natural equilibrium arch. Therefore, the surrounding rock pressure on the roadway roof can be considered to originate solely from the self-weight of the rock mass within the arch[3-7]. The failure range of the roadway sidewalls can be described by the caving angle θ , as expressed in Equation (1)

$$\theta = 45^\circ + \frac{\varphi}{2} \quad (1)$$

In the formula, φ represents the internal friction angle of the rock mass.

The pressure arch is a key theoretical model for analyzing the stability of the surrounding rock of a roadway. The calculation of its parameters requires comprehensive consideration of the mechanical properties of the rock mass and the geometric characteristics of the roadway. Based on Protodyakonov's pressure arch theory and in combination with engineering practice, the key parameters can be calculated using the following formulas:

$$b_1 = l_2 / 2 + h_2 \tan \left(45^\circ - \frac{\varphi}{2} \right) \quad (2)$$

$$h_g = b_1 / f_k \quad (3)$$

$$q_{d\max} = \gamma h_g \quad (4)$$

In the formula: b_1 is half of the span of the pressure arch, m; h_g is the height of the pressure arch, m; $q_{d\max}$ is the maximum vertical pressure acting on the pressure arch, MPa; l_2 is the span of the roadway, m; h_2 is the height of the roadway, m; φ is the friction angle within the rock mass, °; f_k is the Pechmann coefficient.

Based on the Rankine earth pressure theory in soil mechanics, the lateral pressure q_t acting on the roadway side of the pressure arch in the Pechmann surrounding rock pressure arch can be calculated using Equation (4). Estimating the load on the roof of the lower stratum roadway based on the Pechmann pressure arch theory can better reflect the self-supporting arch effect of the overlying rock in the stabilized abandoned area and the surrounding rock pressure transmitted to the roof of the lower stratum roadway.

Since the upper-slice 52113 working face was mined out many years ago, the overlying strata above the goaf have undergone full caving, rotation, and compaction, leaving the caved gangue in a loose accumulation state without an intact rock mass structure. A 1 m thick artificial false roof is left between the lower-slice 52204 working face and the goaf. This top coal, affected by the upper-slice mining, is highly fractured, and its mechanical behavior is closer to that of a granular mass rather than a continuous rock mass. Therefore, the support load is calculated by means of Protodyakonov's pressure arch theory, providing data support for the selection of I-beam sections and the calculation of support spacing.

Based on the geological data of the roof and floor strata of the 5⁻² coal seam in the 52204 working face of the Ulan Cheta Coal Mine and the parameters of the return airway, the Plastik coefficient f_k is taken as 1.8, the roadway width l_2 is 5.0m, the roadway height h_2 is 3.8m, the friction angle within the rock mass φ is 18°, and γ is 14 kPa/m. Due to the influence of mining activities, the roof coal and rock mass within the affected area of the roadway almost has no self-bearing capacity. At this time, the pressure borne by the support body is the self-weight of the roof coal and rock mass.

Assuming that the direct roof of the 5⁻² coal seam (1.3m of siltstone) completely collapses, the calculation yields: the maximum vertical pressure of the pressure arch $q_{d\max} = 40.918$ kPa, and the lateral pressure on the side of the roadway wall $q_{t1} = 49.514$ kPa.

2.2. Return Airway Support Spacing Calculation

The load borne by the supports in the underground roadway[8-11] will vary with the specific conditions of the roadway and the passage of time, taking various forms such as concentrated load, uniformly distributed load, etc., and may manifest as high

top pressure, high side pressure, or high shoulder pressure, etc. Therefore, it is necessary to determine the distribution of the load. To simplify the analysis, it is assumed that the length of the top beam of the rigid metal support is l_a , m; the length of the support leg is l_b , α is the inclination angle of the support leg, and the load concentration of the side beam part is q_b , and the load concentration of the top beam part is q_a . The support constraint conditions are set as follows: the column foot is a fixed hinge support, the connection between the side beam and the top beam is connected by a hinge, as shown in Figure 1.

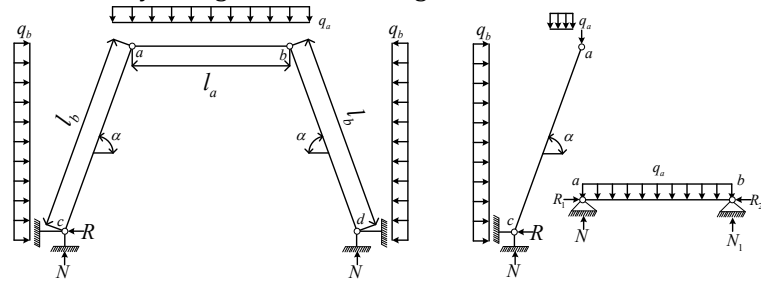


Figure 1. Mechanical Analysis of Rigid Metal Support

In Figure 1, N and R represent the reaction forces, measured in kN, as shown in Equations (6) to (7); the load intensity $q_a = D\sigma y$, $q_b = D\sigma x$, measured in KPa/m; D is the span distance of the I-beam shed, measured in meters.

(1) Calculation of the force on the support leg

$$N = \frac{1}{2} \int_0^{l_a} q_a dx + \int_0^{l_b} q_a \cos \alpha dx \quad (6)$$

$$R = \frac{1}{2} \int_0^{l_a} q_b \sin \alpha dx - \frac{1}{2} \int_0^{l_b} q_b \cot \alpha dy - \frac{1}{2} q_a l_b \cos \alpha \cot \alpha \quad (7)$$

Based on the force equilibrium conditions $\Sigma x = 0$ and $\Sigma y = 0$, as shown in Equations (8) to (9), we obtain:

$$N = N - q_a l_b \cos \alpha \quad (8)$$

$$R = q_b l_b \sin \alpha - R \quad (9)$$

Let p be any section position of the scaffold leg, and the distance from the support foot is l_p ($0 \leq l_p \leq l_b$). Then, the bending moment M_t , shear force Q_t , and axial force T_t of the scaffold leg are shown in Equations (10) to (12):

$$M_t = N l_p \cos \alpha + R l_p \sin \alpha - q_b l_p^2 \sin \alpha / 2 \quad (10)$$

$$Q_t = N \cos \alpha + R \sin \alpha - q_b l_p \sin \alpha \quad (11)$$

$$T_t = N \sin \alpha - R \cos \alpha + q_b l_p \sin \alpha \quad (12)$$

(2) Calculation of the force on the top beam

The bending moment M , deflection y and the maximum tensile stress $\sigma_{d \max}$ at any point x on the top beam are calculated according to Equations (13) to (15):

$$M = (q l_a x - q x^2) / 2 \quad (13)$$

$$y = -q x (l_a^3 - 2 l_a x^2 - x^3) / 24 E I \quad (14)$$

$$\sigma_{d \max} = M_{d \max} / W_z \quad (15)$$

In the formula: q_a represents the uniformly distributed load on the I-beam support, measured in kN/m; l_a represents the net span length of the I-beam support; E represents the elastic modulus of the I-beam; I represents the moment of inertia of the I-beam; M_{dmax} represents the maximum bending moment of the support; W_z represents the flexural section modulus of the support.

Based on the characteristics of the force distribution and the structural properties, it can be known that the maximum bending moment and deflection of the support occur at the midpoint of the support, with the maximum values being M_{dmax} and $|y|_{dmax}$ as shown in Equations (16) to (18):

$$M_{dmax} = q_a l_a^2 / 8 \quad (16)$$

$$|y|_{dmax} = 5q_a l_a^4 / 384EI \quad (17)$$

$$Q_{dmax} = q_a l_a / 2 \quad (18)$$

Substituting the maximum bending moment M_{dmax} of the top beam in Equation (6) into Equation (15), the maximum normal stress σ_{dmax} can be obtained, which represents the pressure q exerted on the top beam, as shown in Equation (19):

$$Q = 8\sigma_{dmax} W_z / l_a^2 \quad (19)$$

In the formula: σ_{dmax} If the yield strength or tensile strength of the top beam is taken, then Q will be the service load or failure load of the top beam.

For the return air roadway using I-beam support, 9th, 11th, and 12th I-beams are proposed to be the main supporting materials for this return air roadway. From the national standard design standards for steel structures, it can be known that the parameters of 9th, 11th, and 12th I-beams are as follows:

Model 9: Bending flexural modulus is 62.5 cm³, yield strength \geq 390 MPa, tensile strength is 570 MPa, elastic modulus is 200 - 210 GPa, moment of inertia is 62.5 cm⁴, axial load range is 85.44 - 89.71 kN. Model 11: Bending flexural modulus is 113.4 cm³, yield strength \geq 335 MPa, tensile strength is 530 MPa, elastic modulus is 200 - 210 GPa, moment of inertia is 127.7 cm⁴, axial load range is 174.56 - 183.29 kN. Model 12: Bending flexural modulus is 144.5 cm³, yield strength \geq 335 MPa, tensile strength is 530 MPa, elastic modulus is 200 - 210 GPa, moment of inertia is 178.2 cm⁴, axial load range is 243.60 - 255.78 kN.

(3) Calculate the spacing of the supports based on the force calculation of the top beam

From the previous text, it is known that the height of the return airway of the 52204 working face of WulanShetai Coal Mine is $h_2 = 3.8\text{m}$ and the span is $l_2 = 5\text{m}$. Under the condition of ignoring the self-weight of the top beam, by substituting the yield strength and tensile strength of the I-beam into Equation (19), the working load Q_{as} and the failure load Q_{dP} of the I-beam can be calculated:

The No. 9 I-beam has a working load of 7.80 kN/m and a failure load of 11.40 kN/m; the No. 11 I-beam has a working load of 12.15 kN/m and a failure load of 19.23 kN/m; and the No. 12 I-beam has a working load of 15.49 kN/m and a failure load of 24.50 kN/m.

By calculating the support spacing of the I-beam support under the working load and failure load, the average value of the two can be taken to obtain the support spacing of the I-beam support. The support spacing D of the I-beam support can be determined by the ratio of the load borne by the I-beam support to the actual coal and rock load, as shown in Equation (20).

$$D = \frac{Q}{q} \quad (20)$$

The calculations show that for the No. 9 I-beam, the support spacing is 190.63 mm under the working load and 278.61 mm under the failure load, giving an average spacing of 234.62 mm; for the No. 11 I-beam, the spacings are 296.94 mm and 469.96 mm, with an average of 383.45 mm; and for the No. 12 I-beam, the spacings are 378.56 mm and 598.76 mm, with an average of 488.66 mm.

(4) Calculation of support spacing based on the force on the support leg

In the same manner as above, the working load Q_{LS} and failure load Q_{LP} for the support legs of different I-beam types are obtained, and the corresponding support spacings are then calculated. The results are as follows:

No. 9 I-beam: The working load is 13.50 kN/m, and the failure load is 19.74 kN/m. No. 11 I-beam: The working load is 21.05 kN/m, and the failure load is 33.30 kN/m. No. 12 I-beam: The working load is 26.82 kN/m, and the failure load is 42.43 kN/m.

For No. 9 I-beam: The support spacing under the working load is 71.48 mm, and the support spacing under the failure load is 104.48 mm, with an average support spacing of 141.82 mm. For No. 11 I-beam: The support spacing under the working load is 111.41 mm, and the support spacing under the failure load is 176.26 mm, with an average support spacing of 231.86 mm. For No. 12 I-beam: The support spacing under the working load is 141.97 mm, and the support spacing under the failure load is 224.60 mm, with an average support spacing of 295.44 mm.

(5) Selection of support spacing

A comparison of the data in Tables 4 and 6 reveals that, for the same type of I-beam under the same loading environment, the support leg spacing is consistently smaller than the roof beam spacing, indicating that the lateral bearing capacity of the support leg is the key factor controlling the support spacing. Laying out the I-beam supports based on the support spacing determined from the force state of the support legs can effectively ensure the structural compatibility between the support legs and the roof beam under the same surrounding rock load, thereby avoiding the risk of premature failure of an individual component due to overloading. Taking the No. 12 I-beam as an example, the average support leg spacing (295.44 mm) is approximately 60% of the average roof beam spacing (488.66 mm). Therefore, the final support spacing should be determined primarily on the basis of the leg calculation results.

Taking both cost and material selection (No. 12 I-beam) into consideration, a dilemma arises in determining the support spacing: adopting a support spacing of $D = 300$ mm satisfies the force requirements of the support legs but constrains

construction efficiency and increases costs; whereas adopting $D = 450$ mm facilitates the roof beam layout but makes it difficult for the support legs to meet the surrounding rock control requirements, posing a considerable risk of leg deformation or failure. To resolve this contradiction and ensure the overall stability of the support system, active supplemental support should be implemented for the sidewall surrounding rock. That is, under a spacing of $D = 450$ mm, sidewall rock bolts are added to compensate for the insufficient support strength of the legs.

2.3. Supplementary support calculation

Rock bolts are additionally installed in the sidewalls of the roadway as a compensatory support measure. On the one hand, the rock bolts enhance the integrity of the sidewall surrounding rock, reducing the risk of support leg instability caused by excessive sidewall deformation; on the other hand, the rock bolts can effectively bear the lateral load transmitted from the return airway, improving the stress state of the support structure and thereby enhancing the overall stability and control performance of the roadway.

When designing rock bolt supplementary support, it is necessary to perform a tensile strength check on the load borne by the rock bolts under lateral pressure. If two or more rock bolts are used in the design, bolts of the same specification should be selected for ease of construction. In this case, the concentrated load acting on the support structure should be reasonably distributed among the individual rock bolts, and a tensile strength check should be carried out for the selected bolt diameter to ensure that the support strength requirements are met. The calculation of the rock bolt support positions is presented below.

$$\begin{aligned}
 q_{t2} &= q_{t1} + P_c \\
 F &= D \int_0^{h_2} q_{t2} dy \\
 D \int_0^{X_0} q_{t2} dy &= (D \int_0^{h_2} q_{t2} dy) / 2 \\
 X_1 &= (D \int_0^{X_0} y q_{t2} dy) / (D \int_0^{X_0} q_{t2} dy) \\
 X_2 &= (D \int_{X_0}^{h_2} y q_{t2} dy) / (D \int_{X_0}^{h_2} q_{t2} dy)
 \end{aligned} \tag{22}$$

where q_{t2} is the sum of the lateral pressure on the pressure arch sidewall q_{t1} and the horizontal load of the boundary coal P_c (kPa); F is the resultant force acting on the coal sidewall of the roadway within the support spacing range (N); X_0 is the segment point of $F/2$ (m); X_1 and X_2 are the equivalent action points of the piecewise function (m); the other variables are as defined above.

After calculation, $F = 323.041$ kN, $X_0 = 2.784$ m, $X_1 = 1.816$ m, $X_2 = 3.315$ m.

When rock bolts are used for sidewall support in the return airway, one, two, or three rock bolts may be adopted as supplementary support. For a single-bolt supplementary arrangement, the bolt is installed at a height of 2.7 m above the floor;

for a two-bolt arrangement, the bolts are installed at heights of 1.8 m and 3.3 m above the floor; and for a three-bolt arrangement, the bolts are installed at heights of 1.8 m, 2.7 m, and 3.3 m above the floor.

A comparative analysis is carried out between the $\phi 18$ non-strengthened 20MnSi threaded steel rock bolt with a yield strength of 53.7 kN and the $\phi 18$ tail-thread-strengthened 20MnSi threaded steel rock bolt with a yield strength of 92 kN, applied in these three supplementary rock bolt configurations. The bending moment of the I-beam support leg is calculated when the supplementary rock bolt reaches its yield load, and the results, together with the case without rock bolt supplementation, are presented in Table 1.

Table 1. Bending Moments of Different Anchor Bolts and Different Compensation Support Frame Legs

Compensation support type	yield load /kN	supporting scheme	Max bending moment of leg/kN·m	Max bending stress/MPa	No. 12 I-beam steel	
					Yield strength	Tensile strength
					335MPa	530MPa
Without rock bolt		Without rock bolt	153.44	1061.87	>	>
$\phi 18$ non-strengthened 20MnSi threaded steel rock bolt	53.7	1 bolt	125.35, 84.27	867.47	>	>
		2 bolts	93.67, 93.66, 34.18	648.24	>	>
		3 bolts	72.01, 62.24, 37.21, 15.02	498.339	>	<
$\phi 18$ tail-thread-strengthened 20MnSi threaded steel rock bolt	92	1 bolt	107.06, 54.41	740.90	>	>
		2 bolts	60.00, 53.50, 8.60	415.22	>	<
		3 bolts	35.53, -2.90, -21.40, -24.20	225.12	<	<

3. Numerical Simulation of Return Airway Support

3.1. Support simulation design

To determine the reasonable support parameters for the 52204 return airway, the FLAC3D numerical simulation method is adopted to analyze the stress evolution and deformation control effect of the surrounding rock under different support schemes and support spacings, thereby providing a basis for the support

design. As indicated in Section 2.1, the return airway is arranged in an inner-stagger layout with an inner stagger distance of 6 m. The model boundary conditions and the physical and mechanical parameters of the rock strata remain consistent with Section 3.3.1. The model dimensions (length \times width \times height) are 300 m \times 10 m \times 72 m. The inner stagger of 6 m is adopted for the subsequent support simulation, and the support schemes are designed as follows:

(1) I-beam support: No. 12 I-beam sets are used, with four support spacings set respectively at 35 cm, 45 cm, 55 cm, and 65 cm.

(2) Combined support of I-beam sets and sidewall rock bolts.

3.2. Analysis of simulation results

(1) Simulation analysis of I-beam support spacing (without rock bolt supplementation)

In the numerical model, displacement monitoring lines were arranged along the strike of the return airway at the midpoints of the roof, left sidewall, and right sidewall. The surrounding rock deformation data under different support spacing conditions were extracted, and the displacement curves were plotted as shown in Fig. 2, to analyze the influence of support parameters on roadway stability.

When the support spacing increases from 35 cm to 65 cm, the roof-to-floor convergence increases from 32.64 mm to 46.63 mm. This indicates that increasing the support density can effectively enhance the bearing capacity of the surrounding rock against vertical loads.

Because the left sidewall deformation of the return airway is primarily governed by a non-uniform stress field, as the support spacing increases, the left sidewall convergence only increases slightly from 75.71 mm to 77.90 mm, with an increment of about 2.2 mm (an increase of 2.9%). This suggests that merely adjusting the support spacing offers limited improvement in the stability of the left sidewall.

It is noteworthy that the right sidewall convergence actually exhibits a decreasing trend with increasing spacing, dropping from 29.13 mm to 26.89 mm, a reduction of approximately 7.7%. This phenomenon may be because a larger support spacing weakens the lateral confinement exerted by the support leg on the goaf side, allowing a partial release of the surrounding rock pressure. Nonetheless, it also indicates that the use of I-beam support alone has a limited ability to restrain the deformation of the right sidewall.

Considering both the support effectiveness and the material consumption during construction, the analysis suggests that a support spacing of 450 mm can achieve a balance between material usage and construction efficiency while satisfying the deformation control requirements of the surrounding rock, and it is therefore identified as the optimal support spacing.

In summary, under the condition of using only I-beam support, the analysis concludes that a support spacing of 450 mm is optimal. The I-beam support alone is

clearly effective in controlling roof and floor deformations, but its control of the two sidewalls is relatively limited. Consequently, the sidewall support needs to be supplemented with other reinforcing measures to achieve the overall stability control of the roadway.

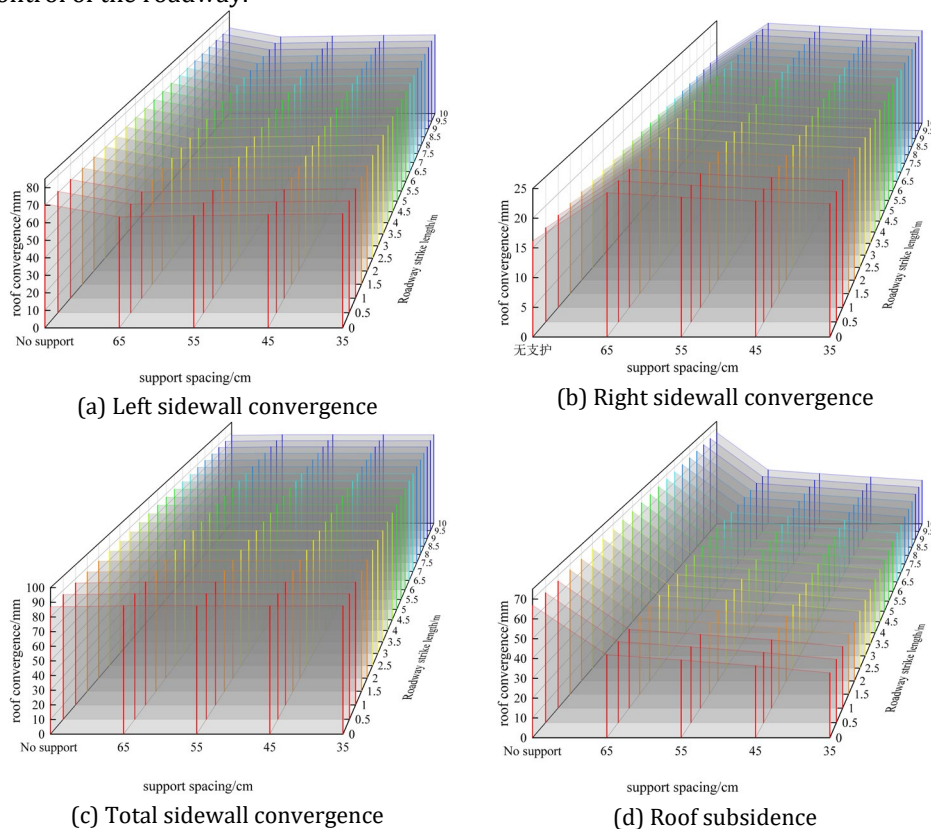


Figure 2. Curve of rock displacement in the roadway supported by I-beam steel (without anchor rod compensation support)

(2) Analysis of support effectiveness

Based on the I-beam support alone described above, sidewall rock bolt supplementary support is added. Lateral monitoring lines were arranged at the same positions in the model, and the surrounding rock deformation data under different support spacings were extracted. The curves of the maximum convergence of the left and right sidewalls versus support spacing are plotted in Fig. 3(a); the curves of the maximum convergence of the roof and the two sidewalls versus support spacing are plotted in Fig. 3(b).

Without rock bolt supplementary support, the maximum roof-to-floor convergence is approximately 36 mm. After adding rock bolt supplementary support, the maximum roof-to-floor convergence increases to around 53 mm. This indicates that adding rock bolts as supplementary support in the return airway alters the stress distribution in the surrounding rock, transferring part of the load to the roof and causing a slight increase in roof deformation. However, regardless of whether 1, 2, or 3 rock bolts are used for supplementary support, the roof convergences of the

three supplementary support schemes are essentially the same, suggesting that the number of supplementary rock bolts has no significant influence on the control of roof subsidence.

Comparing the cases without and with rock bolt supplementary support, the maximum left sidewall convergence decreases from approximately 72 mm (without bolts) to about 44 mm (1 bolt), 38 mm (2 bolts), and 31 mm (3 bolts); the maximum right sidewall convergence decreases from approximately 27 mm (without bolts) to about 13 mm (1 bolt), 11 mm (2 bolts), and 10 mm (3 bolts). The data indicate that the installation of sidewall supplementary rock bolts has a pronounced effect on controlling sidewall deformation. The control effectiveness with 3 bolts is better than that with 2 bolts, which in turn is better than that with 1 bolt.

In summary, the rock bolt supplementary support redistributes the surrounding rock stress and provides a certain degree of control over floor subsidence, although this control effect shows little correlation with the number of supplementary bolts. The best suppression of the two sidewall deformations is achieved with 3 rock bolts as supplementary support. This supplementary support scheme can adequately meet the surrounding rock control requirements of the return airway.

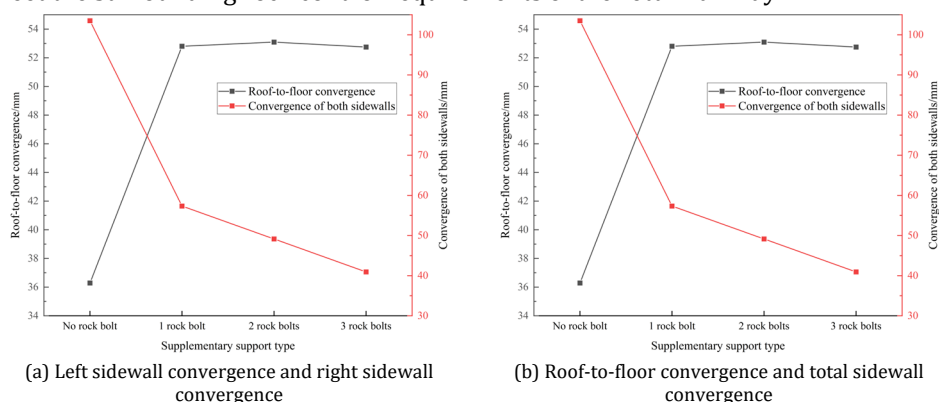


Figure 3. Curve Chart of Surrounding Rock Displacement in Compensated Support Roadway

4. Conclusions

(1) A combined support scheme of “I-beam sets + sidewall rock bolts” is proposed. Based on the principle of adapting to the surrounding rock stress state, No. 12 mine I-beams are selected, with a support spacing of 450 mm, and three ϕ 18 mm non-strengthened 20MnSi threaded steel rock bolts are installed in the sidewall, forming a high-bearing-capacity support structure with active - passive synergy.

(2) The engineering adaptability of the support scheme has been verified. Numerical simulation results show a roof-to-floor convergence of 53 mm and a total convergence of the two sidewalls of 41 mm. The roadway deformation is relatively rapid in the early stage (first 11 days) at rates of 1.7 - 5.2 mm/d, after which it tends to stabilize, indicating that the combined support scheme effectively controls the

surrounding rock deformation.

References

- [1] ZHANG Cun, REN Zhaopeng, HE Jun, et al. Model of overburden pressure arch in mining areas considering thick-hard rock layer and application[J]. *China Mining Magazine*, 2025, 34(03): 113-124+112.
- [2] GE Yang, WANG Hanglong, LI Kegang, et al. Numerical simulation study on overburden strata collapse law of ultra-close goaf based on FLAC3D[J]. *China Mining Magazine*, 2023, 32(02): 97-103.
- [3] CHEN Zhimin, JIANG Yiwen, LI Yazhi, et al. Study on Protodyakonov 's surrounding rock pressure of deep buried tunnel crossing binary stratum[J]. *Chinese Journal of Underground Space and Engineering*, 2024, 20(S2): 582-588.
- [4] SUN Yunjiang, XIE Shengrong, LI Shijun, et al. Reasonable layout and surrounding rock control of roadway in coal pillar area under different horizon key blocks[J]. *Journal of China University of Mining & Technology*, 2016, 45(04): 694-701.
- [5] LI Yanhe, JING Shengguo, TANG Qingteng. Surrounding rock control technology of gob-side entry driving in close-distance coal seams in kilometer deep mine[J]. *Journal of Mining & Safety Engineering*, 2025, 42(03): 613-624.
- [6] WANG Ping, ZENG Zilong, ZHU Yongjian, et al. Principle and technology of surrounding rock control for gob-side entry retaining in ultra-close coal seam group[J]. *Journal of Hunan University of Science & Technology (Natural Science Edition)*, 2024, 39(04): 9-18.
- [7] HOU Yanjuan, ZHANG Dingli, LI Ran, et al. Calculation method for surrounding rock pressure of deeply buried triple-arch tunnel[J]. *Chinese Journal of Theoretical and Applied Mechanics*, 2024, 56(11): 3213-3226.
- [8] YAO Ye, LI Xue, CHEN Meng, et al. Review of researches on the forms and bearing capacities of steel supports for tunnels and roadways[J]. *Metal Mine*, 2025, (11): 200-212.
- [9] CHEN Xinming, GAO Jinhai. Design of secondary powerful support for roadway with high stress, large section and fractured surrounding rock[J]. *Transactions of Beijing Institute of Technology*, 2012, 32(06): 565-570.
- [10] ZHANG Baoyou. Study on layout of staggered roadway and surrounding rock control technology for ultra contiguous coal seams[J]. *Coal Science and Technology*, 2021, 49(08): 88-95.
- [11] ZHANG Junying, YANG Xiaoning, WU Lili. Numerical simulation analysis and field monitoring of support with steel corrugated webs in Baijigou coal mine[J]. *China Mining Magazine*, 2025, 34(06): 224-232.